Bull. Mater. Sci. (2021) 44:221
https://doi.org/10.1007/s12034-021-02496-1

Electronic structure, thermoelectric, mechanical and phonon properties of full-Heusler alloy (Fe_2CrSb): a first-principles study

MANSOUR BENIDRIS[1], ZOUBIR AZIZ[1,*], SHAKEEL AHMAD KHANDY[2], SABRIA TERKHI[1], MUHAMMAD AFTAB AHMAD[3], BOUABDELLAH BOUADJEMI[1], MOHAMMED ABDERRAHIM BENNANI[1] and AMEL LAREF[4]

[1]Laboratory of Technology and Solid's Properties, Abdelhamid Ibn Badis University, 27000 Mostaganem, Algeria
[2]Department of Physics, National Taiwan University, Taipei 10617, Taiwan
[3]Department of Mechanical Engineering, University of Sargodha, Sargodha, Pakistan
[4]Department of Physics and Astronomy, College of Science, King Saud University, Riyadh 11451, Saudi Arabia
*Author for correspondence (zoubir.aziz@univ-mosta.dz)

MS received 20 November 2020; accepted 22 April 2021

Abstract. We hereby discuss the structural stability of Fe_2CrSb via energetic considerations, phonon dynamics and mechanical aspects. Later, the electronic, magnetic and thermoelectric properties are discussed in order to reach out the possible explanations of the observed half-metallic bandgap and other physical properties. Phonon dispersion of Fe_2CrSb with positive-only frequencies accompanied by the observed elastic parameters indicate the dynamic stability and mechaneablity of this alloy. The relaxed and optimized structural calculations predict the ferromagnetic Cu_2MnAl-type L_{21} phase as the stable one. This compound has a half-metallic ferromagnetic character with an integer magnetic moment of 3 μB, which is in good agreement with the Slater–Pauling (SP) rule. Finally, we have pronounced the thermoelectric performance against the temperature range of 50–800 K using Boltzman transport theory. The room temperature Figure of merit (0.54) reaches to maximum of 0.67 at 800 K, indicating that Fe_2CrSb can work at low as well as high temperature thermoelectric devices operations.

Keywords. DFT study; full Heuslers; half-metallicity; electronic and magnetic properties; thermoelectric properties; dynamical and thermo-mechanical stability.

1. Introduction

Full-Heusler compounds are transition metal (TM) and p-group based ternary materials (X_2YZ) with 2:1:1 atomic sequence discovered in 1903 by Friedrich Heusler [1]. The first two elements of this ternary structure (X and Y) are TM atoms and the last one is the III-VIA group atom [2]. If the valence electron count of X atom is higher than Y atom, full-Heusler alloys crystallize in the Cu_2MnAl structure (225-space group); otherwise, they form the Hg_2CuTi phase (216-spacegroup). The four Wyckoff-positions: A (0, 0, 0), B (0.25, 0.25, 0.25), C (0.5, 0.5, 0.5) and D (0.75, 0.75, 0.75) in Cu_2MnAl structure are filled as: X occupies the B and D positions, Y at C and Z at A. In the Hg_2CuTi type, C and D are reserved for X atoms, Y occupies the A position and Z occupies the B position [3–7]. Since their discovery, these materials are intensively investigated for their fascinating applications as topological insulators, superconductive and spintronic materials, thermoelectrics, etc. [8]. De Groot *et al* [9] in 1983 were the first to discover the half-metallicity in NiMnSb. In view of the band structure, this property is described as the semiconducting or insulating character of a material in either of the two spin directions and the metallicity is exhibited in the corresponding spin channel. This makes such kind of compounds as the pronounced candidates for technical applications in spin-injection devices [10], spin-filters [11], tunnel junctions [12] or GMR devices [13]. Among, Fe-based Heuslers, the semiconducting properties of Fe_2TaAl, Fe_2TaGa, Fe_2Val, Fe_2HfSn, Fe_2ZrSi, etc. along with their mechanical and dynamical stability have been probed to achieve large Seebeck coefficients as well as display good thermoelectric performance [14,15]. Yabuuchi *et al* [16] found the power of Fe_2TiSi and Fe_2TiSn to reach 160 μV K^{-1} and the Figure of merit to 0.6. Seebeck coefficients of Fe_2ScP, Fe_2ScAs and Fe_2ScSb compounds are observed to be 770, 386 and 192 μV K^{-1}, respectively, and are recommended to have the possible thermoelectric applicability in wide temperature range [17].

In this study, the physical (e.g., structure, mechanical and phonon stability, electronic, magnetic and transport) properties of Fe_2CrSb alloy are keenly examined using the full-potential linearized augmented plane wave method (FP-LAPW) [18,19], within the generalized gradient

Published online: 27 July 2021

approximation GGA-PBE [20] and TB-mBJ [21–24] approaches to find its usage in several applications, for example spintronics and thermoelectrics. For this, we opted the full-potential based Wien2k code [25], whereas Chen *et al* [26] and Aly *et al* [27] predicted the electronic structure of this material by using Castep [28,29] code and FPLO package, respectively. However, the thermoelectric properties of the full-Heusler Fe_2CrSb viewed as an interesting feature are yet to be explored. Therefore, we discuss the transport coefficients of this material alongside phonon dynamics, electronic properties.

2. Computational details

Ab-initio full-potential linear augmented plane wave (FP-LAPW) method implemented in the Wien2k code is used to carry out the structural optimizations and stability concerns, magneto-electronic and thermoelectric investigations of Fe_2CrSb alloy. We scrutinize the structural stability among the two possible structures, namely, Hg_2CuTi and Cu_2MnAl (see figure 1a). The lattice constants are relaxed and optimized at ambient conditions, where the calculations are done by the GGA-PBE as well as TB-mBJ. Distribution of 2000 k-points with a grid of 12 × 12 × 12 k-mesh in the entire Brillouin zone (BZ) is used, where the cutoff energy is chosen to be –6.0 Ry. The value of $R_{MT} \times K_{max}$ determines the matrix size and was set to 8.0 (where R_{MT} is the smallest of all atomic sphere radii and K_{max} the maximum Kmodulus for the reciprocal lattice vectors).

3. Results and discussions

3.1 *Structure and phonon dynamics*

Birch-Murnaghan's equation of state [30] aided energy optimization has been performed to find the ground-state lattice constants. These calculations were performed for the magnetic phases (ferromagnetic (FM) and non-magnetic (NM)) in the two structural categories of the complete Heusler: Hg_2CuTi and Cu_2MnAl. These two structures are shown in figure 1a and b. The calculation of the variation of the total energy as a function of the volume with GGA-PBE approach has been represented in figure 1c for both structures: Hg_2CuTi and Cu_2MnAl type, and two phases: ferromagnetic (FM) and non-magnetic (NM). From figure 1c, it is clear that the FM configuration of the Cu_2MnAl-type structure is more stable than the Hg_2CuTi-type structure at volume equilibrium because of its lower total energy.

The calculated equilibrium lattice constants a_0, bulk modulus B, its pressure derivative B' and the total energy for Fe_2CrSb are listed in table 1. The lattice parameter corresponding to the equilibrium state is equal to 5.9644 Å. In the absence of experimental results, we compared our predictions to the results found by Chen *et al* [26] and Aly *et al* [27]. This value for lattice constant is in agreement with a difference of less than 1%.

To see the possibility of being able to synthesize this material, we have calculated its formation energy ΔHf per atom at zero temperature by applying the following equation [31]:

$$\Delta H = E_f^{Fe2CrSb} = E_{tot}^{Fe2CrSb} - \left(2 \times E_{Fe}^{bulk} + E_{Cr}^{bulk} + E_{Sb}^{bulk}\right), \quad (1)$$

where $E_{tot}^{Fe2CrSb}$ is the total ground-state energy of Fe_2CrSb per formula unit, and $E_{Fe}^{bulk}, E_{Cr}^{bulk}$ and E_{Sb}^{bulk} are the total ground-state energies of the bulk Fe, Cr and Sb, respectively. The negative value of the formation energy –0.014 Ry implies that Fe_2CrSb can be synthesized [32]. By calculating the cohesive energy, we can again verify the structural stability of the compound. The cohesive energy of a compound X_2YZ is defined as follows:

$$E_{coh}^{X2YZ} = E_{tot}^{X2YZ} - \left(2 \times E_{atom}^{X} + E_{atom}^{Y} + E_{atom}^{Z}\right). \quad (2)$$

Here, E_{tot}^{X2YZ} is the atomic energy of the proposed crystal and $E_{atom}^{X/Y/Z}$ is the energy of X, Y and Z atoms in their fundamental configurations. Replacing X, Y and Z by Fe, Cr and Sb, respectively, in the previous equation, we obtain:

$$E_{coh}^{Fe2CrSb} = E_{tot}^{Fe2CrSb} - \left(2 \times E_{atom}^{Fe} + E_{atom}^{Cr} + E_{atom}^{Sb}\right). \quad (3)$$

All these energies are computed using the GGA-PBE approximation and the observed values are charted in table 2. It is clear from the tabulated data that the negative value of the cohesive energy for Fe_2CrSb compound confirms the structural stability of this material.

The dynamical stability of this material (Fe_2CrSb) is verified by the density functional perturbation theory [33] method, which is utilized to study the dynamics of lattice vibrations in terms of frequency modes of phonons. The phonon frequencies are treated as a second-order derivative of the total energy with respect to atomic translations. We make use of pseudopotential-based Quantum Espresso Package [34] with PBE-GGA approximation for exchange correlations to evaluate these properties. In figure 2, the phonon dispersion curve is plotted and the stable-only phonon modes are found from the positive frequencies. Since Fe_2CrSb possess four atoms in an FCC structure, we can see 12 distinct vibrational modes at any q-point. The 12 vibrational modes constitute 3 acoustic and 9 optical modes.

3.2 *Mechanical properties*

Knowledge of the elastic constants forecasts the reaction of a material against the applied stress. One can also understand different solid-state processes, for example, anisotropic factor, adjacent atomic plane bonding characteristics and structural stability. For the cubic crystal, we need only three independent elastic constants, namely: C_{11}, C_{12} and

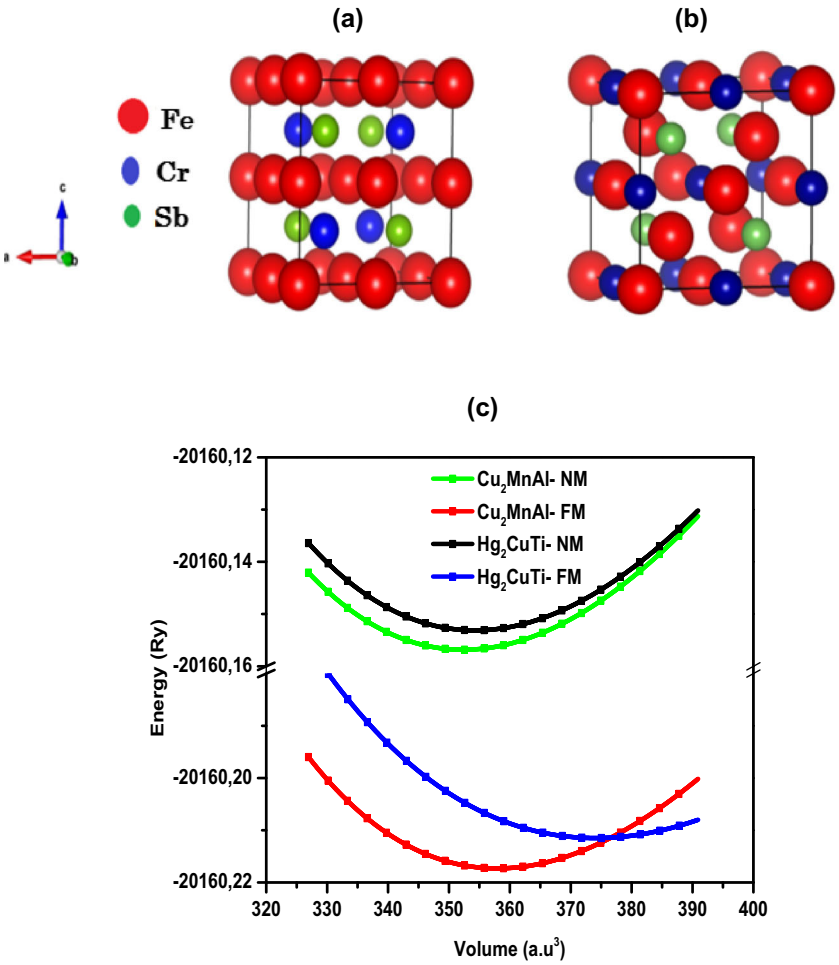

Figure 1. Crystal structure of Fe_2CrSb full-Heusler alloy: (**a**) Cu_2AlMn-type and (**b**) Hg_2CuTi-type structures. (**c**) Calculated total energy as function of the volume for both types of Fe_2CrSb full-Heusler alloy in the two phases ferromagnetic (FM) and non-magnetic (NM) using GGA-PBE approximation.

Table 1. Calculated values of lattice parameter (a_0), bulk modulus B (GPa), its pressure derivative B' and the total energy E_0 for Fe_2CrSb.

			a_0 (Å)	B (GPa)	B'	E_0
Cu_2AlMn type	Our calculations	FM	5.9644	196.3691	4.6894	–20160.217306
		NM	5.9331	210.3136	3.7704	–20160.156831
	Other calculations	CASTEP [26]	5.9400	—	—	—
		FLPO [27]	5.9500	—	—	—
Hg_2CuTi type	Our calculations	FM	6.0526	145.9158	4.0175	–20160.211497
		NM	5.9438	206.7968	3.5250	–20160.153128

Table 2. Calculated formation energy, cohesive energy, atomic energies and ground-state energies of the bulk Fe, Cr and Sb.

	$E_{tot}^{Fe2CrSb}$	E_{Fe}^{bulk}	E_{Cr}^{bulk}	E_{Sb}^{bulk}	E_{atom}^{Fe}	E_{atom}^{Cr}	E_{atom}^{Sb}	$E_f^{Fe2CrSb}$	$E_{coh}^{Fe2CrSb}$
Energies (Ry)	–20160.22	–2545.60	–2101.75	–12967.26	–2545.13	–2101.14	–12967.10	–0.014	–1.717

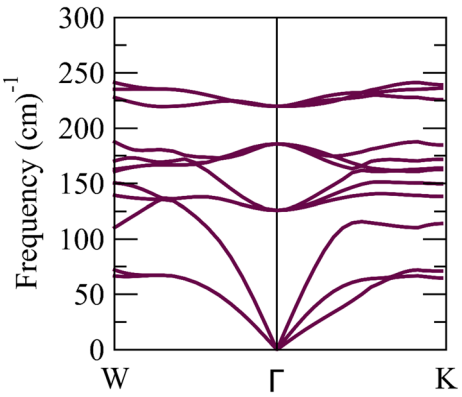

Figure 2. Calculated phonon band structure of Fe_2CrSb full-Heusler alloy in the stable Cu_2AlMn-type structure.

C_{44}. We have calculated these constants for compound Fe_2CrSb in the frame of GGA-PBE at ambient pressure. The obtained results are summarized in table 3. We can see that the stability conditions ($C_{44} > 0$, C_{11}–$C_{12} > 0$, $C_{11}+2C_{12} > 0$, $C_{12} < (C_{11}+2C_{12})/3 < C_{11}$) are satisfied, which ensures and confirm that compound is mechanically stable.

The anisotropic factor (A), bulk modulus (B), shear modulus (G), Young's modulus (E), Poisson's coefficient (v), etc. quantify the response of a crystal towards the external forces and are computed by fitting the calculated elastic constant values in the following equations [35]:

$$A = \frac{2C_{44}}{(C_{11} - C_{12})} \tag{4}$$

$$B = \frac{1}{3}(C_{11} - 2C_{12}) \tag{5}$$

$$G = \frac{1}{2}\left(\frac{C_{11} - C_{12+}3C_{44}}{5} + \frac{5C_{44}(C_{11} - C_{12})}{4C_{44} + 3(C_{11} - C_{12})}\right) \tag{6}$$

$$E = \frac{9BG}{3B + G} \tag{7}$$

$$v = \frac{3B - 2G}{2(3B + G)} \tag{8}$$

From table 3 we notice that the value of the anisotropic factor is different from 1, therefore Fe_2CrSb alloy is anisotropic. Young's modulus finds the stiffness of a crystal; if its value is higher, then the material is considered stiff, else the material is considered ductile. The obtained value shows that our compound is ductile. The ratio between bulk and shear modulus (B/G) is another fundamental parameter regarding the rigidity of materials and the brittle/ductile behaviour. According to Pugh's ratio [36], a material is brittle if $B/G < 1.75$ and ductile if $B/G > 1.75$. Hence, it is clear from the values given in table 3 that Fe_2CrSb is ductile.

Poisson's ratio described as the ratio of transverse strain to the longitudinal strain indicates the stability state against the shear stress and clues the nature of bonding forces between the constituent atoms. Its critical range is 0 to 0.5 [37–39] and for the lower values volume compression occurs and the higher value signify the plasticity of the material; i.e., υ = 0.5 means no volumetric change happened. The obtained value of the Poisson's ratio is 0.27, designates the good plasticity of Fe_2CrSb alloy.

3.3 *Electronic properties*

3.3a *Band profile:* In this study, we describe the electronic properties of Fe_2CrSb by calculating the band structure and the density of states (DOS). Figure 3a and b shows the band structure of Fe_2CrSb calculated within GGA-PBE and the Tran-Blaha modified Becke-Johnson potential (TB-mBJ), respectively. When GGA-PBE and TB-mBJ methods are used, the conduction band minimum (CBM) and the valence band maximum (VBM) are positioned at Γ-X and Γ-W points of symmetry, respectively. Hence, Fe_2CrSb compound has an indirect bandgap of 0.65 eV from PBE and 1.23 eV from TB-mBJ calculations (see table 4). We notice that the results obtained from TB-mBJ scheme are in good agreement with the results obtained by Chen *et al* [26] and Aly *et al* [27]. Furthermore, the spin-up band in figure 3 exhibits metallic character as the VB and CB cross each other over Fermi level, while the minority spin band displays a semiconductor-like gap. Thus, the proposed Fe_2CrSb Heusler presents a half-metallic behaviour. This property likely marks the Fe_2CrSb alloy as appropriate for spintronic applications. From these results, we can conclude that the bandgap calculated by TB-mBJ is more significant than the previous one and more precise because the mBJ scheme handles exchange potential more accurately than PBE functional.

3.3b *Density of states:* The corresponding total (TDOS) and partial (PDOS) density of states for Fe_2CrSb half-

Table 3. Calculated elastic constants C_{11}, C_{12}, C_{44}, bulk modulus (B), shear modulus (G), Young's modulus (E), Poisson's ratio (v), Pugh's ratio (B/G) and anisotropy factor (A) for Fe_2CrSb compound.

	C_{11} (GPa)	C_{12} (GPa)	C_{44} (GPa)	B (GPa)	G (GPa)	E (GPa)	v	B/G	A
Fe_2CrSb	334.46	188.7	187.74	237.33	128.45	326.45	0.23	1.85	2.58

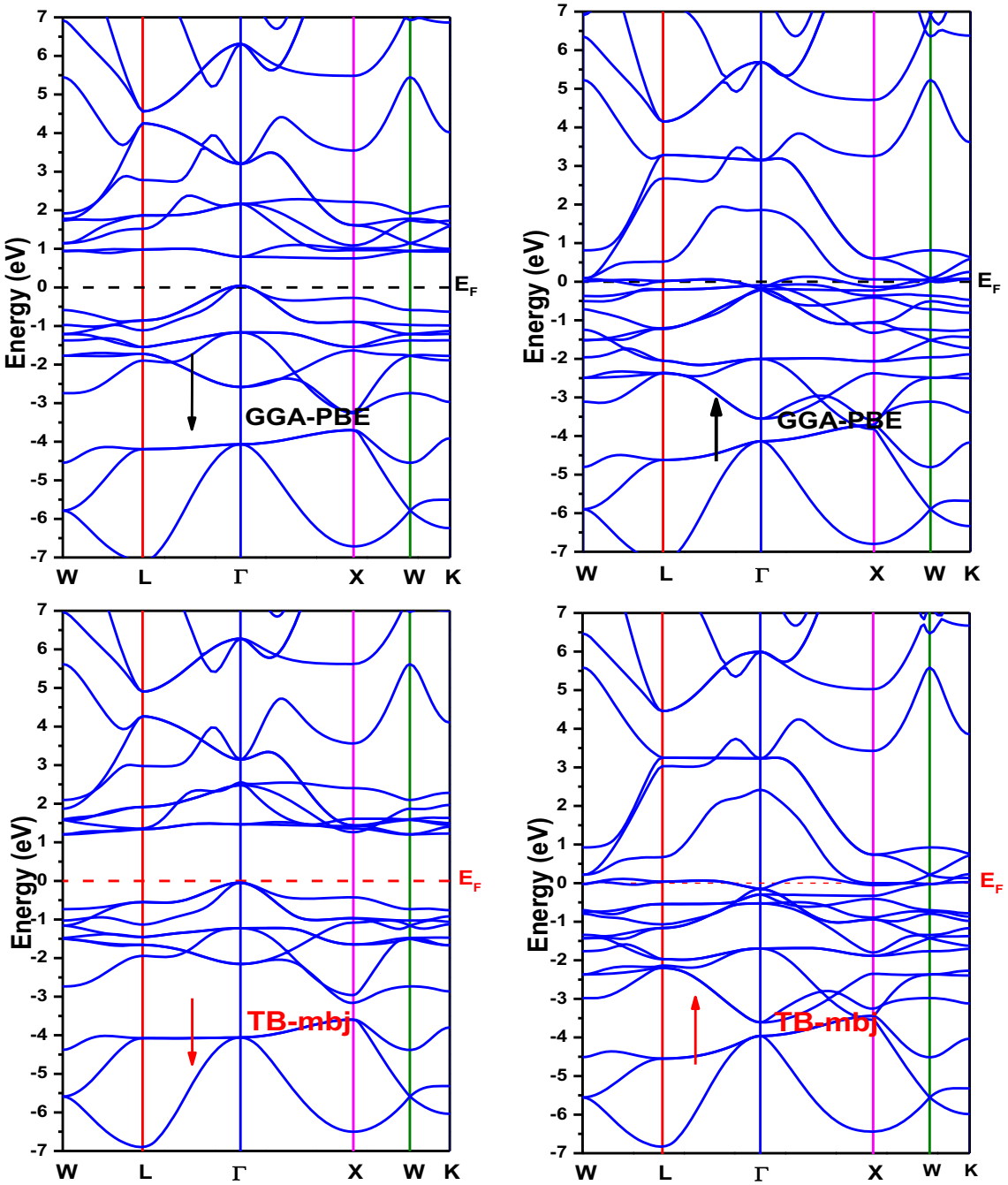

Figure 3. Band structure (majority and minority spin) of Fe_2CrSb compound using GGA-PBE and TB-mBJ.

Table 4. Calculated energy gap E_g (eV) and spin polarization (P) with: GGA-PBE and TB-mBJ approximations.

Compound	Method	E_g (eV)	$\rho\uparrow$	$\rho\downarrow$	$P\%$
Fe_2CrSb	GGA-PBE	0.65	4.98	0	100
	TB-mBJ	1.23	4.57	0	100
	Other calculated [26]	0.56	—	—	—

Heusler compound using GGA-PBE and TB-mBJ are presented in figure 4a and b. The upper part (positive range) of each curve shows the majority spin densities and the lower one (negative range) the minority spin densities. In general, both the curves of TDOS and PDOS are nearly identical with little difference in energy gap at EF for both approximations. According to figure 4, we can see that our system has a very strong magnetic character, this is due to

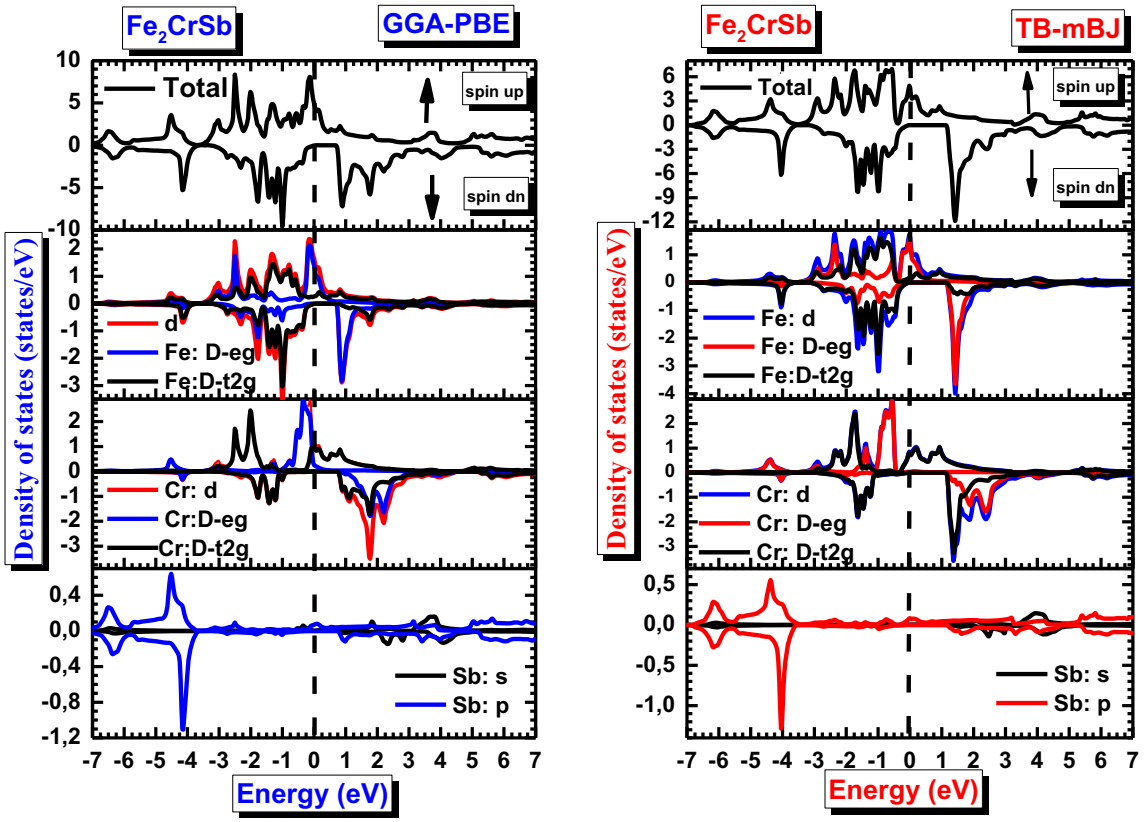

Figure 4. Total and partial densities of states of Fe_2CrSb (up and down) using GGA-PBE and TB-mBJ approximations.

the asymmetry of the majority spin and minority spin states from the TDOS, the half-metallic nature of Fe_2CrSb. Where, the minority spin electronic structure is a semiconductor and the majority spin exhibits the metallic character. This conduction band performance is principally dominated by the contribution of Fe-*3d* and Cr-*3d* states, especially *d-eg* orbitals of both atoms Fe and Cr with a minor contribution from Sb-*4p* states. In the valence band, we can see two regions: the first one ranging from –6.8 to –3.7 eV is mainly occupied by the *4p* orbitals of Sb, and second region between –2.9 and –0.3 eV is dominated by *3d* orbitals of both Fe and Cr atoms. For the conduction band, the robust hybridization between orbital Fe-*3d* and Cr-*3d* states are very clear at –0.2 to –3.5 eV of energy produced by this bandgap. At higher energies (above 5.2 eV), we can see a major contribution of Sb-*4p* with a small impact on Fe-*3d* and Cr-3d states.

To calculate the spin polarization, we use the relation connecting the polarization P with the DOS and by the following relation [40]:

$$P = \frac{\rho\uparrow(E_F) - \rho\downarrow(E_F)}{\rho\uparrow(E_F) + \rho\downarrow(E_F)}, \tag{9}$$

where $\rho\uparrow(E_F)$ and $\rho\downarrow(E_F)$ are the values of majority and minority DOS at Fermi level (E_F). Our calculated values are presented in table 4. It can be seen that Fe_2CrSb alloy shows 100% spin polarization at E_F. The spin-up total DOS has a large positive value at the E_F. However, there is no state at the E_F for the spin-down total DOS. Thus, the full-Heusler Fe_2CrSb in $CuMn_2Al$-type structure alloy exhibits half-metallic behaviour at the equilibrium state.

3.4 *Magnetism and spin moments contribution*

The calculated values of total and partial magnetic moments for Fe_2CrSb, presented in table 5, were evaluated using GGA-PBE and TB-mBJ approximations. It is clear that Cr and Fe atoms with a small contribution of interstitials add the key contribution to the total magnetic moments.

For both approximations (PBE and TB-mBJ), the large positive values of the magnetic spin moment are due to the main contribution of Chromium (2.08 μB) (1.99 μB), while feeble negative values were observed for Antimony (–0.0265 μB) (–0.03151 μB), respectively. This difference of signs indicates the anti-parallel alignment amid the moments of Sb and the other atoms. The integer value of the total magnetic moment per unit cell is one of the consequences of the half-metallic properties of this compound [41]. It equals 3 μB which is in accord with the Slater-Pauling (SP) rule [42] described as $\mu_{tot} = N_v - 24$, where μ_{tot} symbolizes the total spin moment and N_v is the total number

Table 5. Calculated total and partial magnetic moments (in Bohr magneton μB) for Fe_2CrSb compounds with: GGA-PBE and TB-mBJ approximations.

Method	Magnetic moment (μB)				
	μ_{Fe}	μ_{Cr}	μ_{Sb}	$\mu_{interstitial}$	μ_{total}
GGA-PBE	0.44472	2.08560	–0.02651	0.05316	3.00170
mBj-GGA	0.54872	1.99391	–0.03151	–0.05985	2.99999
Other calculated [26]	–0.04	3.18	–0.08	—	3.0000

of valence electrons in a unit crystal [43,44]. For Fe_2CrSb, $N_v = 27$ gives an integral value of magnetic moment and hence advocates the half-metallic ferromagnetism in Fe_2CrSb alloy. Our results of the total magnetic moment were identical to the theoretical results available [26].

3.5 *Thermoelectric properties*

Presently, using thermoelectrics it is possible to recapture some of the waste energy lost into the atmosphere and convert it into electricity. Thermoelectric materials consummate the thermal energy into electrical energy or vice versa and these materials are thus currently used in many industrial applications as power generators or coolers, such as in spacecrafts, electronics, military or medical purposes [45–48]. The efficiency of a thermoelectric material in any power generator or cooler depends on the dimensionless constant $ZT = S^2\sigma T/\kappa$, with S as Seebeck coefficient, σ as electrical conductivity and κ designated as thermal conductivity. BoltzTrap code [49] as executed in the Wien2k code is applied to achieve the ZT and other transport coefficients of Fe_2CrSb material from 50 to 800 K temperature range. We use a denser k-mesh (50 × 50 × 50) to ensure the convergence of transport calculations.

Figure 5 depicts the calculated Seebeck coefficient of the compounds Fe_2CrX (P, As, Sb) as a function of temperature in order to compare the Seebeck coefficient of our material Fe2CrSb by others' materials as Fe_2CrP and Fe_2CrAs. We have seen that all compounds exhibited the positive Seebeck coefficient within the entire temperature range in spin-down state for the entire temperature range for these materials. The Seebeck coefficients were observed as 5.3263, 15.0610 and 155.07 μV K^{-1} for Fe_2CrP, Fe_2CrAs and Fe_2CrSb, respectively (see table 6).

According to these results, the Seebeck coefficient increases as the atomic number of the element X increases. We will take as a convincing example, the comparison between the values of the Seebeck coefficient in spin-down state of the materials Fe_2CrP and Fe_2CrSb, where the value of this coefficient is nearly 29 times more at room temperature (300 K). In fact, the gap width is quite responsive to the lattice parameter and decreases with the expanded lattice (table 2) [26,50]. This can be explained by the increase of the lattice parameter causing the unit cell to expand, which results in the reduction of the bandgap, improving the DOS close to the Fermi level. This decrease in the bandgap leads to an increase in the effective mass of the carriers and consequently the increase in the Seebeck coefficient in accordance with the simplified Mott relation [51,52].

$$S = \frac{8\pi^2 K_B^2}{3eh^2} m^* T \left(\frac{\pi}{3n}\right)^{2/3},$$

where m^* is the effective mass of the charge carriers, K_B the Boltzmann constant, e the elementary charge, h the Plank constant, n the concentration of charge carriers and T the absolute temperature.

We can conclude that Fe_2CrSb material has a large Seebeck coefficient at room temperature in spin-down state compared to the spin-up state than Fe_2CrX(P, As). Therefore a certain interest for thermoelectric applications.

The electrical conductivities per relaxation time (σ/τ) *vs.* temperature are shown in figure 6a for both spin directions. For both states of spin (up and down), the electrical conductivity increases almost linearly with the temperature, passing from the value 160 × 10^{18} $(\Omega ms)^{-1}$ at 50 K to 185 × 10^{18} $(\Omega ms)^{-1}$ at 800 K in the spin-up state. However for the spin-down state, the values of the electrical conductivity per relaxation time are spread between 2.98 × 10^{18} $(\Omega ms)^{-1}$ at 50 K and 9.48 × 10^{18} $(\Omega ms)^{-1}$ at 800 K. These results show a very high electrical conductivity, although lower in the spin-down state confirming the semi-conductive nature of this material in this spin state. Therefore, a very low resistivity of this material and a consequent transport of electric charges with very low losses by the Joule effect, which represents a major advantage for being a good thermoelectric material. At room temperature (300 K), the value of electrical conductivity per relaxation time in the spin-down state is equal to 4.32 × 10^{18} $(\Omega ms)^{-1}$. The thermal conductivity is sum of electron contribution and lattice vibrations such as $K = K_e + K_l$, where the K_e and K_l are the electronic part (electrons and holes transporting heat) and lattice vibrations part (phonon contribution), respectively. The variation of the thermal conductivity per relaxation time against temperature (κ_e/τ, electronic part only) for both spin channel is shown in figure 6b. It can be clearly observed from these curves that in the spin-up state, the thermal conductivity (κ_e/τ) increases linearly from 1.93 × 10^{14} (W K^2 m s)$^{-1}$at 50 K to 4.29 × 10^{15} (W K^2 m s)$^{-1}$ at

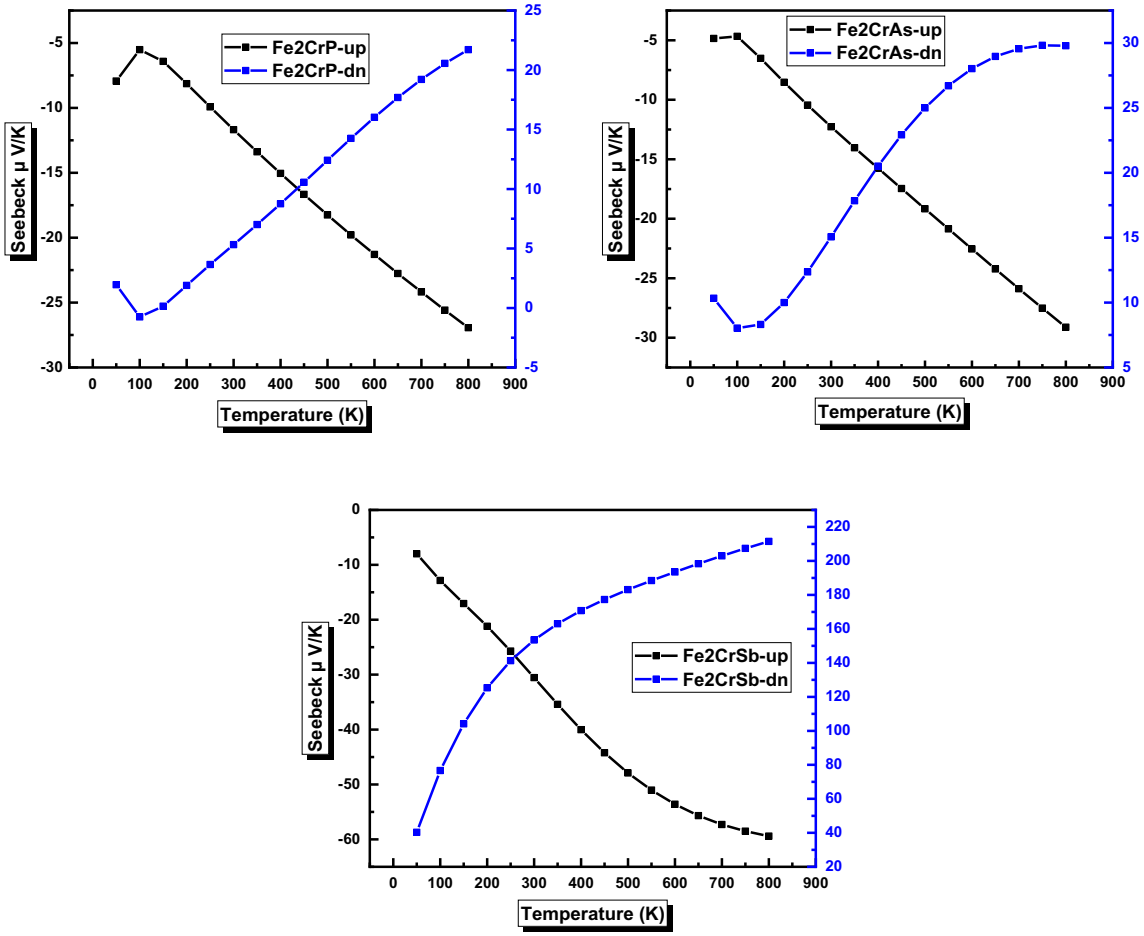

Figure 5. Seebeck coefficient of Fe_2CrX (X = P, As, Sb) as a function of temperature.

Table 6. Values of the Seebeck coefficient in the two spin states at different temperatures and energy gap of the alloys Fe_2CrX (X = P, As, Sb).

	S (μV K^{-1})					
	Fe_2CrP		Fe_2CrAs		Fe_2CrSb	
Alloy	Spin up	Spin down	Spin up	Spin down	Spin up	Spin down
T = 50 K	–7.93794	1.9582	–4.8492	10.3352	–7.992	40.2897
T = 300 K	–11.6792	5.3263	–12.2728	15.0610	–30.545	155.07
T = 800 K	–26.9387	21.7106	–29.1166	29.7899	–59.410	211.470
Energy gap (eV)	0.79		0.71		0.65	

800 K. While for the spin-down channel, we can see the non-linear variation of the electronic thermal conductivity, increasing from 4.18×10^{12} (W K^2 m s)$^{-1}$ at 50 K to 5.06×10^{14} (W K^2 m s)$^{-1}$ at 800 K. At room temperature, the values of the thermal conductivity (κ_e/τ) are about 1.35×10^{15} (W K^2 m s)$^{-1}$ and 5.62×10^{13} (W K^2 m s)$^{-1}$ for spin-up and spin-down states, respectively. It should be noted that the electrical and thermal conductivity plots look very similar, these results are in accordance with the Wiedemann-Franz law, which states the proportional relationship between these two quantities as follows: $K = \sigma LT$, where L is the Lorenz number; σ represents the electrical conductivity, while T is the absolute temperature. In figure 6c, we have plotted the parameter data synthesizing the efficiency of thermoelectric devices for the Fe_2CrSb material in the two spin states (up and down) as a function of the temperature, it is Figure of merit (ZT). The Figure of merit (ZT) provides the performances of a thermoelectric

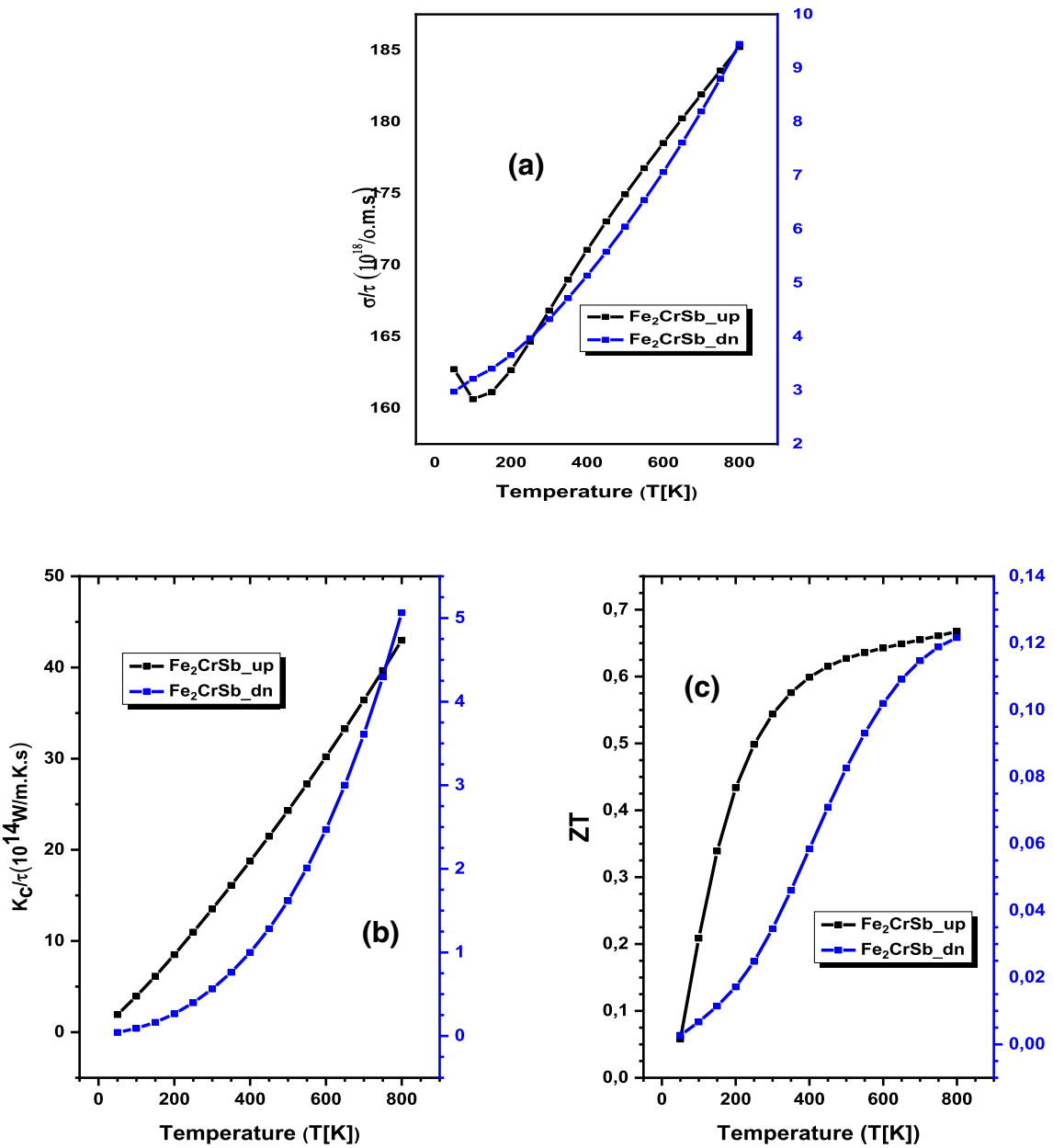

Figure 6. Thermoelectric transport properties of Fe_2CrSb as a function of temperature; (**a**) electrical conductivity (σ/τ); (**b**) Thermal conductivity ($\kappa e/\tau$) and (**c**) thermoelectric Figure of merit (ZT).

material and the capacity of a given material to efficiently produce thermoelectric power. For both states of spin (up and down), the curves are quite similar, i.e., the Figure of merit (ZT) increases almost linearly with increase in temperature and reaches its maximum value (ZT_{max} = 0.125 and 0.68 (800 K) for spin-up and spin-down states, respectively. Then they become practically constant at higher temperature (above 600 K). ZT reaches a value of nearly 0.54 and 0.68 at 300 and 800 K, respectively, in the spin-down channel, which is very considerable compared to the available thermoelectric materials [16]. Keeping in view the above thermoelectric results, we conclude that Fe_2CrSb shows a remarkable thermoelectric performance in the spin-down state, accompanied by a significant value of ZT greater than that of many full-Heuslers reported till date. We cannot compare our results due to shortage of experimental or theoretical results; however, these simulations can be considered as reference data for future endeavors.

4. Conclusion

In summary, we have successfully performed the first-principles calculations to probe the structural, electronic, magnetic, elastic and thermoelectric properties of Fe_2CrSb Heusler alloy. The study of structural properties revealed

that Fe_2CrSb compound is energetically more stable in $CuMn_2Al$-type structure FM state. The negative value for the enthalpy of formation confirms that the compound can be synthesized and is stable thermodynamically. By calculating the cohesive energy, we can again corroborate the structural stability of our compound. Phonon dispersion curve with no imaginary frequencies pledges the dynamical stability of this alloy. The band structure confirms an indirect bandgap in minority spin at the Γ-X point (0.65 eV) for GGA-PBE and 1.23 eV at the Γ-X points for TB-mBJ approximation. The electronic and magnetic properties reveal that Fe_2CrSb compound has a half-metallic ferromagnet behaviour. The elastic properties govern the mechanical stability of the present Heusler alloy, which is anisotropic and ductile in nature. Our thermoelectric study predicts Fe_2CrSb as a probable thermoelectric material with considerable values of a Figure of merit at low and high temperatures. Finally, the investigated properties suggest the application of this material in thermoelectric devices and spintronic applications.

Acknowledgements

We would like to acknowledge the General Director of Scientific Research (GDST), Algeria, for providing financial support to conduct this study. AL acknowledges the Research Center of Female Scientific and Medical Colleges, Deanship of Scientific Research, King Saud University, for the financial support.

References

[1] Khandy S A and Chai J D 2021 *J. Alloys Compd.* **850** 156615
[2] Sakuma A 2002 *J. Phys. Soc. Jpn.* **71** 2534
[3] Tas M, Şaşıoğlu E, Friedrich C and Galanakis I 2017 *J. Magn. Magn. Mater.* **441** 333
[4] Hirohata A, Frost W, Samiepour M and Kim J 2018 *J. Mater.* **11** 105
[5] Sato K and Saitoh E 2015 *Spintronic for next generation innovative devices* (Chichester, West Sussex, United Kingdom: John Wiley & Sons Inc.)
[6] Kandpal H C, Fecher G H and Felser C 2007 *J. Phys. D: Appl. Phys.* **40** 1507
[7] Graf T, Fesler C and Parkin S S P 2011 *Prog. Solid State Ch.* **39** 1
[8] Chatterjee S, Das S, Pramanick S, Chatterjee S, Giri S, Benerjee A *et al* 2019 *J. Magn. Magn. Mater.* **478** 155
[9] De Groot R A, Mueller F M, van Engen P G and Buschow K H J 1983 *Phys. Rev. Lett.* **50** 2024
[10] Hossain A, Rahman M T, Khatun M and Haque E 2018 *Comput. Condens. Matter* **15** 31
[11] Heusler F 1903 *Verh. Dtsch. Phys. Ges.* **12** 219
[12] Felser C and Hirohata A 2016 *Springer series in Materials Science* **222** 401
[13] Kara H, Upadhyay Kahaly M and Özdoğan K 2018 *J. Alloys Compd.* **735** 950e958
[14] BilcI D, Hautier G, Waroquiers D, Rignanese G M and Ghosez P 2015 *Phys. Rev. Lett.* **114** 13660
[15] Khandy S A, Ishtihadah I, Gupta D C, Bhat M A, Shabir A, Dar T A *et al* 2018 *RSC Adv.* **8** 40996
[16] Yabuuchi S, Okamoto M, Nishide A, Kurosaki Y and Jun Hayakawa J 2013 *J. Appl. Phys. Express.* **6** 025504
[17] Sharma S and Pandey S K 2014 *J. Phys. D: Appl. Phys.* **47** 445303
[18] Rozale H, Khetir M, Amar A, Lakja A, Sayede A and Benhelal O 2014 *J. Superlattice Microst.* **74** 146
[19] Schreiber E, Anderson O L and Soga N 1973 *Elastic constants and their measurements* (New York: Mc Graw-Hill) p 40
[20] Voigt W 1928 Lehrbuch der Kristallphysik (Leipzig: Teubner) 739
[21] Reuss A and Angew Z 1929 *Math. Mech.* **9** 49
[22] Ustundag M, Aslan M and Yalcin B G 2014 *Comput. Mater. Sci.* **81** 471
[23] Chenine D, Aziz Z and Benstaali W 2018 *J. Supercond. Nov. Magn.* **31** 285
[24] Schwarz K and Blaha P 2003 *Comput. Mater. Sci.* **28** 259
[25] Blaha P, Schwarz K, Madsen G K H, Kvasnicka D and Luitz J 2001 *WIEN2k, An augmented plane wave plus local orbitals program for calculating crystal properties* (Austria: Techn. Universitat Wienna)
[26] Chen B S, Li Y Z, Guan X Y, Wang C, Wang C X and Gao Z Y 2015 *J. Supercond. Nov. Magn.* **28** 1559
[27] Aly S H and Shabar R M 2014 *J. Magn. Magn. Mater.* **360** 143
[28] Segall M D, Lindan P J D, Probert M J, Pickard C J, Hasnip P J, Clark S J *et al* 2002 *J. Phys. Condens. Matter* **14** 2717
[29] Payne M C, Teter M P, Allen D C, Arias T A and Joannopoulos J D 1992 *Rev. Mod. Phys.* **64** 1045
[30] Murnaghan F D 1944 *Proc. Natl. Acad. Sci. USA* **30** 244
[31] Karimian N and Ahmadian F 2015 *Solid State Commun.* **223** 60
[32] Hautier G, Ong S P, Jain A, Moore C J and Ceder G 2012 *Phys. Rev. B* **85** 155208
[33] Giannozzi P, Baroni S, Bonini N, Calandra M, Car R, Cavazzoni C *et al* 2009 *J. Phys. Condens. Matter* **21** 395502
[34] Gonze X, Allan D C and Teter M P 1992 *Phys. Rev. Lett.* **68** 3603
[35] Khandy S A, Islam I, Kaur K, Nazir A A and Laref A 2020 *Phys. B: Condens. Matter* **578** 411839
[36] Pugh S F 1954 *Phil. Mag.* **45** 43
[37] Kaur K and Kumar R 2017 *J. Alloys Compd.* **727** 1171
[38] Ghosh S and Gupta D C 2016 *J. Magn. Magn. Mater.* **411** 120
[39] Kaur K 2017 *J. Europhys. Lett.* **117** 47002
[40] Soulen Jr R J, Byers J M, Osofsky M S, Nadgorny B, Ambrose T, Cheng S F *et al* 1998 *Science* **282** 85
[41] Galanakis I, Dederichs P H and Papanikolaou N 2002 *Phys. Rev. B* **66** 174429
[42] Zheng N and Jin Y 2012 *J. Magn. Magn. Mater.* **324** 3099
[43] Birsan A 2014 *J. Curr. Appl. Phys.* **14** 1434
[44] Zener C 1951 *Phys. Rev.* **82** 403
[45] Rowe D M 2006 *Thermoelectrics Handbook: Macro to Nano* (1st edn) (Boca Raton, FL: CRC Press), https://doi.org/10.1201/9781420038903
[46] Su X, Wei P, Li H, Liu W, Yan Y, Li P *et al* 2017 *Adv. Mater.* **29** 1602013
[47] Zheng G, Su X, Xie H, Shu Y, Liang T, She X *et al* 2017 *Energy Environ. Sci.* **12** 2638
[48] Khandy S A and Chai J D 2020 *J. Appl. Phys.* **127** 165102

[49] Madsen G K and Singh D J 2006 *Comput. Phys. Commun.* **175** 67
[50] Picozzi S, Continenza A and Freeman A J 2006 *Phys. Rev. B* **66** 094421
[51] Bhardwaj A, Misra D K, Pulikkotil J J, Auluck S, Dhar A and Budhani R C 2012 *Appl. Phys. Lett.* **101** 133103
[52] Chen S and Zhifeng R 2013 *Mater. Today* **16** 387